Geochemical Characteristics of Siqueiros Transform, East Pacific Rise

Yao Y Yan, John F Casey

(South Florida Water Management District, West Palm Beach, FL 33406, USA;
Geosciences Department, University of Houston, Houston, TX 77204, USA)

Abstract: Basalts recovered from the Siqueiros transform exhibit a wide compositional range from primitive to evolved compositions. The most primitive samples collected from strike-slip fault A-B, have the highest MgO contents up to 14.91 wt%. The most evolved samples with lower MgO content were collected from the western ridge-transform intersection. Three classes of MORBs are distinguished in the transform domain: E-MORBs, Primitive N-MORBs and N-MORBs. Two mantle sources are identified in the Siqueiros region. One is the enriched mantle with highest REEs, enriched LREEs, low MgO, K_2O and TiO_2 and high $^{87}Sr/^{86}Sr$ isotopic concentrations, which lies underneath the western part of the transform domain. The second source is the depleted mantle, which lies underneath the mid-eastern transform domain. Basalts from this source have low $^{87}Sr/^{86}Sr$ isotopic compositions, lower REEs and trace elements and higher contents.

Key words: MORB; basalts; geochemistry; mantle source tracers; Siqueiros transform; East Pacific Rise
中图分类号: P541; P591+2; P736;　　**文献标识码:** A　　**文章编号:** 1672-4135(2006)04-0279-15

1 Introduction

Transform faults separating mid-oceanic ridge (MOR) segments comprise a principal type of plate boundary, and their effects on the generation of the ocean crust are of fundamental importance. Variations in structural trends along active transforms provide key evidence for recent plate reorganizations, and small changes in fracture zone azimuth indicate older periods of plate readjustment. Geophysical and geological investigations have demonstrated that the ocean crust is thin proximal to ridge/transform intersections (Fox et al., 1981; Stroup & Fox, 1981; Detrick & Purdy, 1980). The existence of thin ocean crust led to the idea that the juxtaposition of a cold edge of lithosphere might affect processes of basalt generation at the ridge/transform plate boundary (Fox, 1978; Gallo & Fox, 1979; Stroup & Fox, 1981; Bonatti & Honnorez, 1976). Melson & Thompson (1971) are among the first to compare the petrologic differences in basalts found in transform faults with basalts erupted along ridges. Hekinian and Thompson (1976) found that basalts from transforms tend to be more fractionated than basalts elsewhere on ridges. Bender et al. (1983) examined the Tamayo fracture zone which is located at the mouth of the Gulf of California at 23° N and connects the East Pacific Rise (EPR) with the Gulf Rise. They found there were distinct chemical differences between basalt glass samples collected far from the Tamayo Transform ('swell samples') and close to the transform/ridge intersection ('rift samples').

The Siqueiros transform is about 20 km wide, and lies between 8° 20'N and 8° 30'N, offsetting the East Pacific Rise (EPR) axis by 138 km in a left-lateral sense (Fig. 1 INSET). The slip rate along this Ridge-Transform-Ridge (RTR) boundary is approximately 63 km/Ma (half-rate) (Fig. 1). This study focus on geochemical studies of basalts and basalt glasses from Siqueiros transform region, East Pacific Rise (EPR). Multibeam bathymetric data collected in the Siqueiros-Alvin Diving Cruise (May 2 to June 2, 1991) was also processed using GIS software to describe the topographic and tectonic features in Siqueiros area. Four intra-transform spreading centers and five strike-slip faults were well constrained (Fig. 1).

收稿日期: 2006-10-12
基金项目: 美国国家科学基金的海洋钻探子项目(This research was part of the Ocean Drilling Program (ODP) funded by the U.S. National Science Foundation")
作者简介: 颜耀阳(1964-),男,在读博士,高级地理信息研究员,主要从事地理信息科学、遥感、地质、空间信息模演及地质统计分析,E-mail: yyan@sfwmd.gov。

2 Geochemistry of Basaltic Rocks

Young volcanism occurs in some transform domains, especially those transforms offsetting fast- and superfast-spreading portions of Mid-Oceanic Ridge (MOR) crest. Transform volcanism occurs either at intra-transform spreading centers or at small, eruptive centers in transform shear zones. A series of dives and dredges collected hundreds of samples covering the Siqueiros transform domain and its intersections with adjacent East Pacific Rise (Fig. 1, Table 1).

During the Alvin Cruise, three broad categories of erupted lavas from the spreading centers were described: aphyric basalt, plagioclase phyric basalt, and plagioclase/olivine phyric basalt. All of these have a significant degree of vesicularity. A total of 39 dredges and 5 rock cores were also obtained during the cruise. Perfit et al. (1996) conducted a preliminary study of the geochemical characteristics of young picritic basalts from within the A-B strike-slip fault and associated N-MORB lavas recovered from the western portion of the transform domain. One hundred and seven dredge samples are analyzed for bulk rock major, trace, and rare elements by the Inductively Coupled Plasma (ICP) Spectrometry at the University of Houston. Sample preparation for analysis of major, trace and rare earth elements by ICP is the same as described by Smith (1994).

2.1 Major elemental geochemical characteristics within Siqueiros transform domain

In order to examine the major element geochemical variations of the transform domain, glass and whole rock data are compiled from previously published work and from our unpublished data. Data are grouped based on their specific tectonic locations and geochemical differences: western ridge-transform intersection (W. RTI), intra-transform spreading centers (ITSCs) (A, B), intra-transform strike-slip faults (A-B, B-C), western transform domain (including spreading centers C and D, and strike-fault C-D) and eastern tip of the East Pacific Rise (E. T. EPR).

Western ridge-transform intersection (W.RTI): Samples come from dive 2 390 that covers the small ridge that connects EPR to south wall of A-B fault. The whole-rock analyses show evolved compositions with MgO contents of 5.54 ~ 6.37 wt%, Mg values of 44 ~ 55 (Mg value = {(MgO/40.32)/ [MgO/40.32+0.85*Fe_2O_3(T)/71.85]}*100), CaO/Al_2O_3 ratios of 0.67 ~ 0.74, SiO_2/Fe_2O_3(T) ratios of 3.57 ~ 4.72, Na_2O contents of 2.84 ~ 3.01 wt%, Fe_2O_3(T) content of 10.4 ~ 14.02. Hig hest contents of TiO_2 contents (2.47 wt%, 2.84 wt %) and K_2O contents (0.3 wt% and 0.73 wt %) (Table 2 and Fig. 2).

ITSC A: Samples come from dredges D38, D35, D36 and dives 2 386 and 2 389. Whole-rock analyses are primitive to moderately fractionated with MgO contents of 7.20 ~ 9.60 wt%, Mg values of 56 ~ 70, CaO/Al_2O_3 ratios of 0.65 ~ 0.89, SiO_2/Fe_2O_3 (T) ratios of 4.27 ~ 5.66, Na_2O contents of 2.08 ~ 2.73 wt%, Fe_2O_3 (T) content of 8.93 ~11.32 wt%. Low contents of K_2O (0.02 ~ 0.12 wt %) and TiO_2 (0.93 ~ 1.76 wt %) (Table 2 and Fig. 2).

ITSC B: The whole-rock analyses from dives 2375, 2376, 2380 and dredges D1, D25, D26, D27 have uniform compositions with MgO contents of 6.10 ~ 8.40 wt%, Mg values of 54 ~ 66 (most are between 56 ~ 64, and sample D4-8 has Mg value of 72), CaO/Al_2O_3 ratios of 0.72 ~ 0.91 (0.64 of D25-110 and 0.63 of 2 382-10wr), SiO_2/Fe_2O_3(T) ratios of 3.57 ~ 4.71, Na_2O contents of 2.39 ~ 3.10 wt% and Fe_2O_3(T) contents of 9.12 ~ 12.08 wt%. Intermediate contents of TiO_2 (1.12 ~ 1.97 wt %) and low to intermediate K_2O contents (0.055 ~ 0.293 wt%) (Table 2 and Fig. 2).

Strike-slip fault A-B:Samples from A-B fault can be divided into two groups based on their compositional differences as designated as group A-B(E) (enriched) and group A-B(P) (primitive) (Table 2 and Fig. 2).

A-B (E):whole-rock analyses from dives 2384, 2379 and dredges D17, D20 and D38 show evolved basaltic compositions with MgO contents of 6.52 ~ 8.53 wt%, Mg values of 52 ~ 66, CaO/Al_2O_3 ratios of 0.66 ~ 0.82, SiO_2/Fe_2O_3(T) ratios of 3.72 ~ 5.39, Na_2O contents of 2.46 ~ 3.02 wt%, Fe_2O_3(T) contents of 9.35 ~ 13.18 wt%. Intermediate TiO_2 contents (1.3 ~ 2.41 wt %), high K_2O contents (0.11 ~ 0.31 wt%).

A-B (P):Whole-rock samples mainly come from dive 2384 and dredges D20, D22, D23 and D24 that covered the central portion of the A-B fault. Most of them are picritic and olivine-phyric basalts. Their compositions are exclusively primitive with MgO contents of 8.79 ~ 14.91 wt%, Mg values of 67 ~ 78,

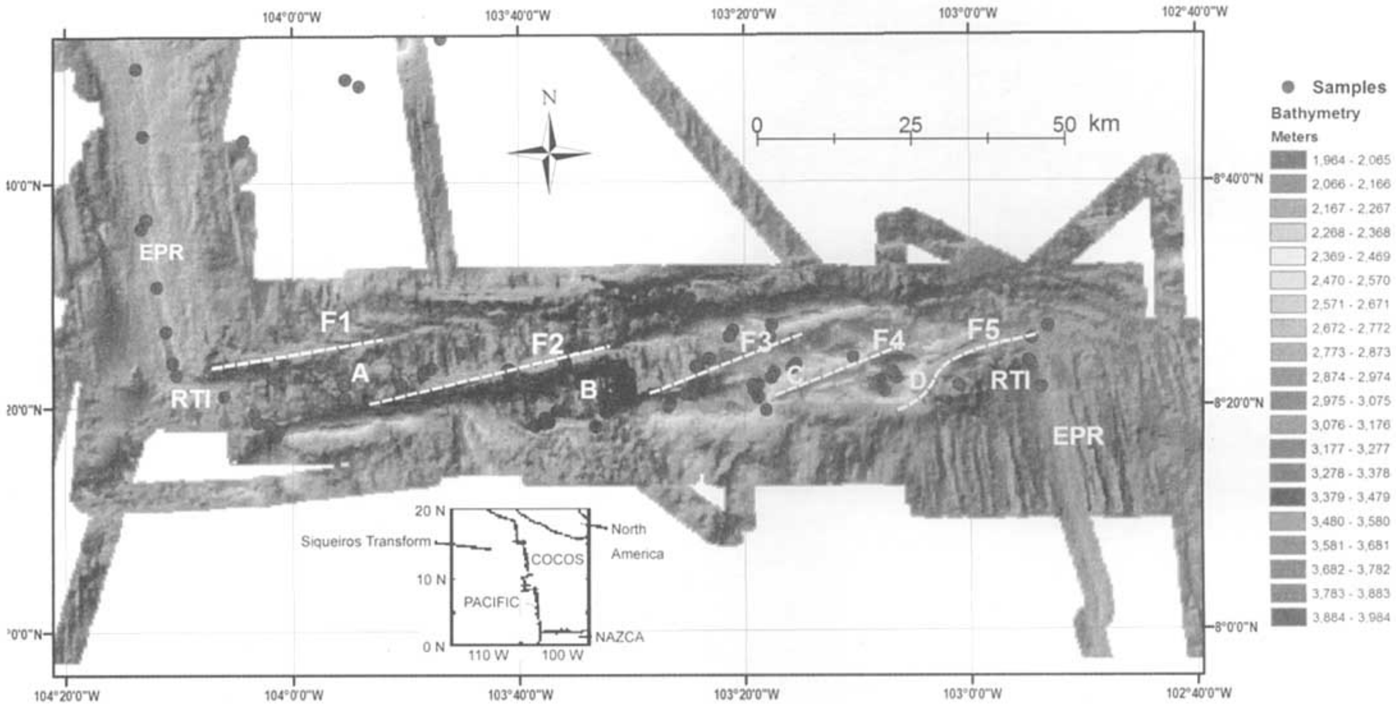

Fig. 1 Shaded relief map of bathymetry shows the morpho-tectonics and sample locations of Siqueiros transform and adjacent East Pacific Rise

图 1 Siqueiros 转换断层及其附近的东太平洋洋隆的海测地形、地貌构造及采样位置

The INSET shows the study location; EPR: East Pacific Rise; A, B, C and D: intra-transform spreading centers; F1-F5: strike-slip faults connecting western EPR, spreading centers A, B, C, D and eastern EPR, respectively; RTI: ridge-transform intersection

图中插图示研究范围; EPR:东太平洋洋隆;A、B、C、D:转换断层内的扩张中心;F1–F5: 连接东太平洋洋隆的西端、扩张中心 A、B、C、D 和东太平洋洋隆东端的走滑断层;RTI: 洋脊 – 转换断层交会处

Table 1 Sample Locations and Tectonic Settings

表1 样品地点及其构造环境

SampleID	Latitude	Longitude	Setting	Source*	Method	SampleID	Latitude	Longitude	Setting	Source*	Method
176565	8.3661	-103.84	A	a	XRF	177084	8.3811	-103.6764	A-B(P)	a	XRF
178606	8.395	-103.9567	A	a	XRF	177114	8.3828	-103.6772	A-B(P)	d	XRF
D38-1	8.3667	-103.9233	A	a	XRF	176810	8.3744	-103.6594	A-B(P)	d	XRF
D38-100	8.3667	-103.9233	A	a	ICP	176839	8.3706	-103.6617	A-B(P)	a	XRF
D38-101	8.3667	-103.9233	A	a	ICP	176931	8.3708	-103.6694	A-B(P)	a	XRF
D38-102	8.3667	-103.9233	A	a	ICP	2384-7a	8.3739	-103.6717	A-B(P)	a	XRF
D38-103	8.3667	-103.9233	A	a	ICP	2384-7b	8.3739	-103.6717	A-B(P)	a	XRF
D38-110	8.3667	-103.9233	A	a	ICP	176992	8.3756	-103.6728	A-B(P)	a	XRF
D38-111	8.3467	-103.9233	A	a	ICP	177023	8.3778	-103.6739	A-B(P)	a	XRF
D38-112	8.3467	-103.9233	A	a	ICP	D20-1	8.3483	-103.6483	A-B(P)	a	XRF
D38-113	8.3467	-103.9233	A	a	ICP	D20-15	8.36	-103.655	A-B(P)	a	XRF
D38-114	8.3467	-103.9233	A	a	ICP	D20-2	8.3483	-103.6483	A-B(P)	a	ICP
D38-115	8.3467	-103.9233	A	a	ICP	D20-3	8.3483	-103.6483	A-B(P)	a	ICP
D38-122	8.3467	-103.9233	A	a	ICP	D20-30	8.36	-103.655	A-B(P)	a	ICP
D38-2	8.3667	-103.9233	A	a	XRF	D20-4	8.3483	-103.6483	A-B(P)	a	ICP
TW74-D3	8.4	-103.94	A	a	XRF	D20-5	8.3483	-103.6483	A-B(P)	a	XRF
176445	8.3578	-103.835	A	a	XRF	D20-5®	8.3483	-103.6483	A-B(P)	a	ICP
D35-3	8.39	-103.795	A	a	XRF	D20-6	8.355	-103.6483	A-B(P)	a	ICP
D35-4	8.3833	-103.8067	A	a	XRF	D20-7	8.355	-103.6483	A-B(P)	a	ICP
D36-3	8.4133	-103.75	A	a	XRF	D20-8	8.355	-103.6483	A-B(P)	a	ICP
CHEPR-64	8.382	-104.17	A-B	c	XRF	D22-2	8.375	-103.6617	A-B(P)	a	XRF
TW74-D6	8.35	-103.65	A-B	a	XRF	D22-3	8.375	-103.6617	A-B(P)	a	XRF
TW74-D7	8.38	-103.68	A-B	a	XRF	D22-4	8.375	-103.6617	A-B(P)	a	XRF
2379-2WR	8.3906	-103.6	A-B(E)	a	XRF	D23-1	8.3833	-103.6733	A-B(P)	a	ICP
2384-13	8.3861	-103.6789	A-B(E)	d	XRF	D23-2	8.375	-103.6692	A-B(P)	a	XRF
2384-14	8.3883	-103.6806	A-B(E)	d	XRF	D24-B	8.3867	-103.6833	A-B(P)	a	ICP
2384-4a	8.37	-103.6622	A-B(E)	a	XRF	174223	8.3931	-103.5206	B	a	XRF
D17-10	8.3983	-103.5983	A-B(E)	a	ICP	174496	8.3653	-103.5161	B	a	XRF
D17-102	8.3983	-103.5983	A-B(E)	a	ICP	174527	8.3639	-103.0153	B	a	XRF
D17-103	8.3983	-103.5983	A-B(E)	a	ICP	174254	8.3917	-103.5183	B	a	XRF
D17-107	8.3983	-103.5983	A-B(E)	a	ICP	174282	8.3922	-103.5153	B	a	XRF
D17-109	8.3983	-103.5983	A-B(E)	a	ICP	174313	8.3894	-103.5189	B	a	XRF
D17-11	8.3983	-103.5983	A-B(E)	a	ICP	174343	8.3878	-103.5228	B	a	XRF
D17-114	8.3983	-103.5983	A-B(E)	a	ICP	174374	8.3819	-103.5225	B	a	XRF
D17-122	8.3983	-103.5983	A-B(E)	a	ICP	174435	8.3694	-103.5178	B	a	XRF
D17-126	8.3983	-103.5983	A-B(E)	a	ICP	D1-21	8.345	-103.5367	B	a	ICP
D17-136	8.3983	-103.5983	A-B(E)	a	ICP	D1-22	8.345	-103.5367	B	a	ICP
D17-138	8.4117	-103.5983	A-B(E)	a	ICP	D1-23	8.345	-103.5367	B	a	ICP
D17-141	8.4117	-103.5983	A-B(E)	a	ICP	D1-24	8.345	-103.5367	B	a	ICP
D17-146	8.4117	-103.5983	A-B(E)	a	ICP	D1-25	8.345	-103.5367	B	a	ICP
D17-149	8.4117	-103.5983	A-B(E)	a	ICP	D1-26	8.345	-103.5367	B	a	ICP
D17-151	8.4117	-103.5983	A-B(E)	a	ICP	D1-27	8.3367	-103.5333	B	a	ICP
D17-154	8.4117	-103.5983	A-B(E)	a	ICP	D1-28	8.3367	-103.5333	B	a	ICP
D17-155	8.4117	-103.5983	A-B(E)	a	ICP	D1-29	8.3367	-103.5333	B	a	ICP
D17-157	8.4117	-103.5983	A-B(E)	a	ICP	D1-30	8.3367	-103.5333	B	a	ICP
D17-159	8.4117	-103.5983	A-B(E)	a	ICP	D1-31	8.3367	-103.5333	B	a	ICP
D17-160	8.4117	-103.5983	A-B(E)	a	ICP	D1-32	8.3367	-103.5333	B	a	ICP
D17-192	8.4117	-103.5983	A-B(E)	a	ICP	D1-33	8.3367	-103.5333	B	a	ICP
D17-1WR	8.3167	-103.6283	A-B(E)	a	XRF	D1-34	8.345	-103.5367	B	a	ICP
D20-148	8.37	-103.66	A-B(E)	a	ICP	D1-5	8.345	-103.5367	B	a	XRF
D20-160	8.37	-103.66	A-B(E)	a	ICP	D4-1	8.3767	-103.5067	B	a	ICP
D20-163	8.37	-103.66	A-B(E)	a	ICP	D4-100	8.38	-103.5033	B	a	ICP
D20-164	8.37	-103.66	A-B(E)	a	ICP	D4-11	8.38	-103.5033	B	a	ICP
D20-165	8.37	-103.66	A-B(E)	a	ICP	D4-12	8.38	-103.5033	B	a	ICP
176779	8.3756	-103.6583	A-B(P)	a	XRF	D4-2	8.3767	-103.5067	B	a	ICP
177053	8.3789	-103.675	A-B(P)	d	XRF	D4-4	8.3767	-103.5067	B	a	ICP

continued(续表 1)

SampleID	Latitude	Longitude	Setting	Source*	Method	Sample_ID	Latitude	Longitude	Setting	Source*	Method
RAIT 02-	8.39	-103.52	B	a	XRF	D19-1	8.3083	-103.6283	B	a	XRF
D25-100	8.4033	-103.385	B	a	ICP	D19-2	8.3617	-103.4083	B	a	XRF
D25-103	8.4033	-103.385	B	a	ICP	D8-1	8.3267	-103.6	B	a	XRF
D25-109	8.3917	-103.405	B	a	ICP	D8-1(R)	8.3267	-103.6	B	a	ICP
D25-110	8.3917	-103.405	B	a	ICP	175988	8.3517	-103.42	B-C	a	XRF
D25-112	8.3917	-103.405	B	a	ICP	2381-3A	8.3383	-103.4417	B-C	a	XRF
D25-116	8.3917	-103.405	B	a	ICP	177875	8.3667	-103.3767	B-C	a	XRF
D25-119	8.4033	-103.385	B	a	ICP	177906	8.36	-103.3883	B-C	a	XRF
D25-6	8.445	-103.35	B	a	XRF	177995	8.3583	-103.3992	B-C	a	XRF
D26-101	8.445	-103.35	B	a	ICP	178026	8.35	-103.4083	B-C	a	XRF
D26-102	8.445	-103.35	B	a	ICP	D2	8.355	-103.4108	B-C	a	ICP
D26-104	8.445	-103.35	B	a	ICP	D2-5	8.355	-103.4067	B-C	a	ICP
D26-106	8.445	-103.35	B	a	ICP	D28-1	8.3667	-103.38	B-C	a	ICP
D26-107	8.4367	-103.355	B	a	ICP	174619	8.365	-103.3117	C	a	XRF
D26-108	8.4367	-103.355	B	a	ICP	174739	8.3567	-103.3183	C	a	XRF
D26-109	8.4367	-103.355	B	a	ICP	174769	8.3267	-103.3	C	a	XRF
D26-110	8.4367	-103.355	B	a	ICP	177176	8.365	-103.32	C	a	XRF
D26-113	8.4367	-103.355	B	a	ICP	2385-3a	8.3617	-103.315	C	a	XRF
D26-123	8.4367	-103.355	B	a	ICP	2385-6t	8.3467	-103.3117	C	a	XRF
D26-128	8.4533	-103.2917	B	a	ICP	D32-1	8.3817	-103.2883	C	a	XRF
D27-100	8.4533	-103.2917	B	a	ICP	D32-2	8.3817	-103.2883	C	a	ICP
D27-106	8.4533	-103.2917	B	a	ICP	D32-3	8.375	-103.2933	C	a	XRF
D27-107	8.4533	-103.2917	B	a	ICP	D32-3 (R	8.375	-103.2933	C	a	ICP
D27-108	8.4367	-103.295	B	a	ICP	D32-5	8.375	-103.2933	C	a	ICP
D27-114	8.4367	-103.295	B	a	ICP	D32-6	8.375	-103.2933	C	a	ICP
D27-130	8.4367	-103.295	B	a	ICP	D33-1	8.395	-103.2567	C	a	XRF
D27-132	8.4367	-103.295	B	a	ICP	D33-2	8.39	-103.2617	C	a	ICP
D27-133	8.4533	-103.2917	B	a	ICP	D33-3	8.39	-103.2617	C	a	ICP
D27-5	8.3667	-103.38	B	a	XRF	D34-2	8.405	-103.1717	C-D	a	XRF
D4-6	8.3767	-103.5067	B	a	XRF	177630	8.355	-103.125	D	a	XRF
D4-6(R)	8.3767	-103.5067	B	a	ICP	177691	8.37	-103.1333	D	a	XRF
D4-8	8.3767	-103.5067	B	a	ICP	D44-1	8.3833	-103.1133	D	a	XRF
D4-9	8.3767	-103.5067	B	a	ICP	D44-2	8.375	-103.1067	D	a	ICP
D4-UHB	8.3767	-103.5067	B	a	ICP	CHEPR-61	8.36	-102.893	E.T.EPR	c	XRF
175592	8.345	-103.5	B	a	XRF	D30-1	8.4333	-102.9067	E.T.EPR	a	XRF
175623	8.3417	-103.495	B	a	XRF	D30-1(R)	8.4333	-102.9067	E.T.EPR	a	ICP
175653	8.3417	-103.495	B	a	XRF	D30-3	8.4	-102.9117	E.T.EPR	a	ICP
175378	8.3617	-103.5142	B	a	XRF	D30-4	8.4	-102.9117	E.T.EPR	a	ICP
175409	8.3617	-103.5142	B	a	XRF	D30-5	8.4	-102.9117	E.T.EPR	a	ICP
175439	8.3583	-103.5067	B	a	XRF	D30-6	8.4	-102.9117	E.T.EPR	a	ICP
175500	8.3583	-103.5067	B	a	XRF	D31-1	8.45	-102.8833	E.T.EPR	a	ICP
175562	8.345	-103.5	B	a	XRF	RAIT 02-	8.33	-103.02	E.T.EPR	a	XRF
173673	8.35	-103.5433	B	a	XRF	CHEPR-63	8.446	-104.185	W.RRI	c	XRF
173735	8.33	-103.5303	B	a	XRF	178971	8.325	-104.055	W.RTI	a	XRF
174162	8.3461	-103.5225	B	a	XRF	2390-3A	8.31	-104.05	W.RTI	a	XRF
173888	8.3672	-103.5217	B	a	XRF	2390-3B	8.31	-104.05	W.RTI	a	XRF
173917	8.3644	-103.5219	B	a	XRF	179061	8.3067	-104.0333	W.RTI	a	XRF
173978	8.3578	-103.5194	B	a	XRF	179091	8.2983	-104.03	W.RTI	a	XRF
174009	8.35	-103.5178	B	a	XRF	179152	8.291	-104.0233	W.RTI	a	XRF
174039	8.3472	-103.5178	B	a	XRF	179183	8.2983	-104.02	W.RTI	a	XRF
174070	8.3486	-103.5208	B	a	XRF	179214	8.2983	-104.02	W.RTI	a	XRF
174101	8.3444	-103.5206	B	a	XRF	CHEPR-67	8.4	-104.175	W.RTI	c	XRF
2382-10w	8.325	-103.5383	B	a	XRF	RAIT 02-	8.35	-104.1	W.RTI	a	XRF
176230	8.3033	-103.5533	B	a	XRF	SD-8	8.378	-104.028	W.RTI	c	XRF
D18-1WR	8.31	-103.6217	B	a	XRF	TW74-D8	8.37	-104.02	W.RTI	a	XRF
D18-3	8.305	-103.6433	B	a	XRF						

Sources*: a: This study; c: Petrology Database: East Pacific Rise Data Synthesis, Section IX, compiled by Langmuir, 1988; d: Perfit et. al. (1996)

CaO/Al_2O_3 ratios of 0.62 ~ 0.76, SiO_2/Fe_2O_3 (T) ratios of 4.72 ~ 6.29, Na_2O contents of 2.16 ~ 2.68 wt% and Fe_2O_3(T) contents of 7.64 ~ 9.81 wt%. Lowest contents TiO_2 (0.84 ~1.18 wt %) and K_2O (0.0013 ~ 0.07 wt %) (Table 2 and Fig. 2).

Strike-slip faults B-C and C-D: Whole-rock analyses for B-C from dives 2 387, 2381 and 2387, dredges D2 and D28 have fractionated composition with MgO contents of 6.66 ~ 8.43 wt%, Mg values of 54 ~ 64, CaO/Al_2O_3 ratios of 0.77 ~ 0.80, SiO_2/Fe_2O_3 (T) ratios of 3.67 ~ 5.29, Na_2O contents of 2.34 ~ 3.02 wt%, Fe_2O_3(T) contents of 9.48 ~ 13.19 wt%. Only one sample available from fault C-D (D43-2) has a little primitive composition with MgO content of 9.12 wt%, Mg value of 68, CaO/Al_2O_3 ratio of 0.80, SiO_2/Fe_2O_3(T) ratio of 5.76, Na_2O content of 2.06 wt%, Fe_2O_3(T) content of 8.65 wt%. Intermediate contents of TiO_2 (1.02 ~ 2.04 wt%) and K_2O (0.01 ~ 0.27 wt%) (Table 2 and Fig. 2).

ITSCs C and D: Both C and D have similar compositions with MgO contents of 7.34 ~ 8.43 wt% and 7.99 ~ 8.23 wt%, Mg values of 58 ~ 65 and 62~65, CaO/Al_2O_3 ratios of 0.78 ~ 0.87 and 0.82 ~ 0.85, SiO_2/Fe_2O_3(T) ratios of 4.22 ~ 5.50 wt% and 4.70 ~ 5.76, Na_2O contents of 2.34 ~ 2.98 wt% and 2.30 ~ 2.46 wt%, Fe_2O_3 (T) contents of 9.14 ~ 11.46 wt% and 9.34 ~ 10.77 wt%, respectively. Intermediate contents of TiO_2 (1.02~2.04 wt %) and K_2O (0.01 ~ 0.27 wt %) (Table 2 and Fig. 2).

E.T.EPR: Whole rock samples from dredges D31 and D30 show uniform compositions with MgO contents of 6.75 ~ 7.54 wt%, Mg values of 56 ~ 59, CaO/Al_2O_3 ratios of 0.81 ~ 0.85, SiO_2/Fe_2O_3(T) ratios of 4.04 ~ 4.29, Na_2O contents of 2.68 ~ 3.27 wt% and Fe_2O_3(T) contents of 11.77 ~ 12.43 wt% (Table 2 and Fig. 2). Interme- diate contents of TiO_2 (1.70 ~ 1.97 wt %) and K_2O (0.11 ~ 0.18 wt %).

2.2 Variations of major elemental geochemistry within the transform

Basalts recovered from dives and dredges from the Siqueiros transform domain exhibit a wide compositional range from primitive to evolved compositions. The Mg content was used to illustrate differentiation from primitive to more evolved composition (Schilling, 1975). A value of Mg # of 70 defines a basaltic magma in equilibrium with mantle olivine, and primitive glass and whole-rock compositions amongst the spectrum of erupted MORB are rare. Relatively fractionated magmas are dominant, indicating that the primary MORB magmas may have undergone high-level fractionation after segregation from their mantle sources.

From whole-rock data, the most primitive samples were collected from strike-slip fault A-B (P) (dredge D20 — D23 and dive 2384) with highest Mg values of 67 ~ 78 and highest MgO contents up to 14.91 wt%. There are also some primitive samples from spreading center A (D38-100 ~ 111), and rarely from B (D4-8) and C-D. There is only one sample from fault C-D and it is primitive with Mg value of 68 (Fig. 2). The most evolved samples were collected from western ridge-transform intersection with smaller Mg values of 44 and 55 (two samples), and low MgO content of 5.54 and 6.37 wt%. In terms of major element parameters sensitive to the extent of partial melting, samples from W.RTI and some from B have the highest Na_2O contents (2.84 ~ 3.27 wt%) and lowest CaO/Al_2O_3 ratio (< 0.70). Samples from fault A-B(P), some samples from spreading centers A, B, C, and D, fault B-C, and the one sample from fault C-D have the lowest Na_2O contents (1.99 ~ 2.50 wt%). All other samples, including most samples from spreading centers A, B, C, and D, faults A-B(E) and B-C, and Eastern tip of the EPR, have intermediate to high Na_2O contents (2.5 ~ 3.0 wt%). As we see from these diagrams, the biggest compositional variation occurs within the A-B fault, ranging from very primitive to well-evolved compositions. This is very similar to the case in Hayes transform, where the largest compositional range is observed from the Hayes transform valley (Smith et al, 1994). Relatively fractionated magma compositions are dominant, indicating that the primary MORB magmas must have undergone high-level fractionation after segregation from their mantle source (Table 2 and Fig. 2).

3 Trace and Rare-earth Element Geochemistry

Basalts from mid-oceanic ridges were classified into three groups based on the trace and rare earth characteristics. N-MORB are LREE-depleted (e.g. low $(La/Sm)_{cn}$ and $(La/Yb)_{cn}$ ratios), incompatible element-depleted (e.g., low Cs, Rb, K, Ba, Sr, Ti, Zr, Nb abundances) and have low $^{87}Sr/^{86}Sr$ ratios. E-MORB (enriched) are considered to be LREE-enriched ($(La/Sm)_{cn}>2.0$), incompatible element-enriched, and exhibit higher $^{87}Sr/^{86}Sr$ ratios. Transitional basalts or T-MORBs exhibit intermediate $(La/Sm)_{cn}$ ratios of 0.8 ~ 2.0

Table 2 Major Elemental Composition Summary
表 2 主要元素成分一览

SETTING	STATS	SiO_2	Al_2O_3	TiO_2	MnO	Na_2O	Fe_2O_3T	MgO	CaO	K_2O	P_2O_5	TOTAL
W.RTI												
(2)*	Avg	49.49	14.14	2.66	0.23	2.93	12.21	5.96	9.92	0.52	0.4	98.43
	Min	48.97	12.87	2.47	0.18	2.84	10.4	5.54	9.47	0.3	0.32	98.38
	Max	50.01	15.4	2.84	0.27	3.01	14.02	6.37	10.37	0.73	0.48	98.48
A												
-19	Avg	49.74	15.42	1.27	0.19	2.31	10.14	8.44	12.08	0.06	0.11	99.76
	Min	46.72	14.36	0.93	0.16	2.03	8.93	7.35	11.26	0.02	0.08	98.66
	Max	51.04	17.9	1.76	0.24	2.73	11.35	9.55	12.88	0.12	0.18	100.69
A-B(E)												
-30	Avg	49.91	15.19	1.77	0.17	2.68	11.11	7.33	11.53	0.2	0.16	99.98
	Min	48.67	14.11	1.3	0.13	2.28	9.35	6.52	10.53	0.11	0.11	98.37
	Max	51	16.68	2.41	0.23	3.02	13.18	8.53	12.4	0.31	0.22	100.98
A-B(P)												
-27	Avg	48.7	16.78	0.99	0.12	2.31	8.43	10.86	11.67	0.03	0.07	100.02
	Min	45.1	15.05	0.84	0.09	1.99	7.64	8.79	10.64	0	0.04	99.13
	Max	50.06	18.28	1.18	0.16	2.68	9.81	14.91	12.22	0.13	0.1	100.86
B												
(62)\	Avg	50.01	15.02	1.52	0.18	2.7	10.73	7.6	11.92	0.15	0.14	99.98
	Min	47.75	14.25	1.13	0.15	2.29	8.9	6.12	9.73	0.05	0.08	98.48
	Max	52.74	19.21	2.15	0.25	3.1	12.36	10.42	13.58	0.29	0.25	100.99
B-C												
-6	Avg	49.87	14.86	1.62	0.21	2.71	11.1	7.38	11.65	0.13	0.14	99.66
	Min	48.45	13.62	1.35	0.16	2.34	9.48	6.66	10.72	0.03	0.1	98.65
	Max	50.55	16.12	2.04	0.26	3.02	13.19	8.43	12.66	0.27	0.21	100.46
C												
-14	Avg	50.32	14.89	1.36	0.19	2.71	10.39	7.71	12.07	0.08	0.11	99.82
	Min	49.54	14.13	1.12	0.17	2.34	9.14	7.34	11.7	0.01	0.06	98.88
	Max	51.02	15.62	1.58	0.22	2.98	11.74	8.43	12.41	0.16	0.13	100.9
C-D												
-1		49.86	16.28	1.02	0.12	2.06	8.65	9.12	12.96	0.06	0.05	100.2
D												
-4	Avg	50.76	14.91	1.17	0.19	2.38	10.02	7.99	12.35	0.05	0.08	99.91
	Min	50.65	14.64	1.07	0.12	2.3	9.34	7.52	11.88	0.02	0.07	99.61
	Max	50.94	15.18	1.31	0.27	2.46	10.77	8.23	12.72	0.08	0.09	100.43
E.T.EPR												
-6	Avg	50.07	14.26	1.79	0.19	2.78	12.03	7.24	11.78	0.16	0.15	100.45
	Min	48.87	13.94	1.7	0.17	2.58	11.77	6.75	11.36	0.11	0.14	99.48
	Max	50.81	14.55	1.97	0.2	3.27	12.43	7.54	12.08	0.28	0.18	100.94

*number of samples

(Schilling et. al., 1983;Bryan et al., 1976; Sun et al., 1979; le Roex et al., 1983, 1985; Langmuir, et al., 1992).

3.1 Trace and rare-earth elemental geochemical characteristics of basalts within the transform

Western RTI: Basalts in this area have (169.4 ~ 180.2) × 10^{-6} Zr (with exception that sample 2390-7 has 111.80 Zr), (226 ~ 269) × 10^{-6} Cr and (120 ~ 304) × 10^{-6} Sr. The ratios of Zr/Y, Ti/Zr and K/Ti are 3.39 ~ 5.61, 74.62 ~ 94.02, and 0.11 ~ 0.40, respectively. Most samples from this RTI have typical LREE-enriched patterns, and have $(La/Sm)_{cn}$ values of 1.70 ~ 1.93 and $(La/Yb)_{cn}$ values of 2.82 ~ 3.14. Two samples (2390-7 and 2390-9) are slight LREE-depleted, and have $(La/Sm)_{cn}$ and $(La/Yb)_{cn}$ ratios of 0.66 ~ 0.75 and 0.79 ~ 0.87, respectively. Based on the definition defined above, most samples from this area are E-MORBs, and some are N-MORBs (Table 3, Fig. 3).

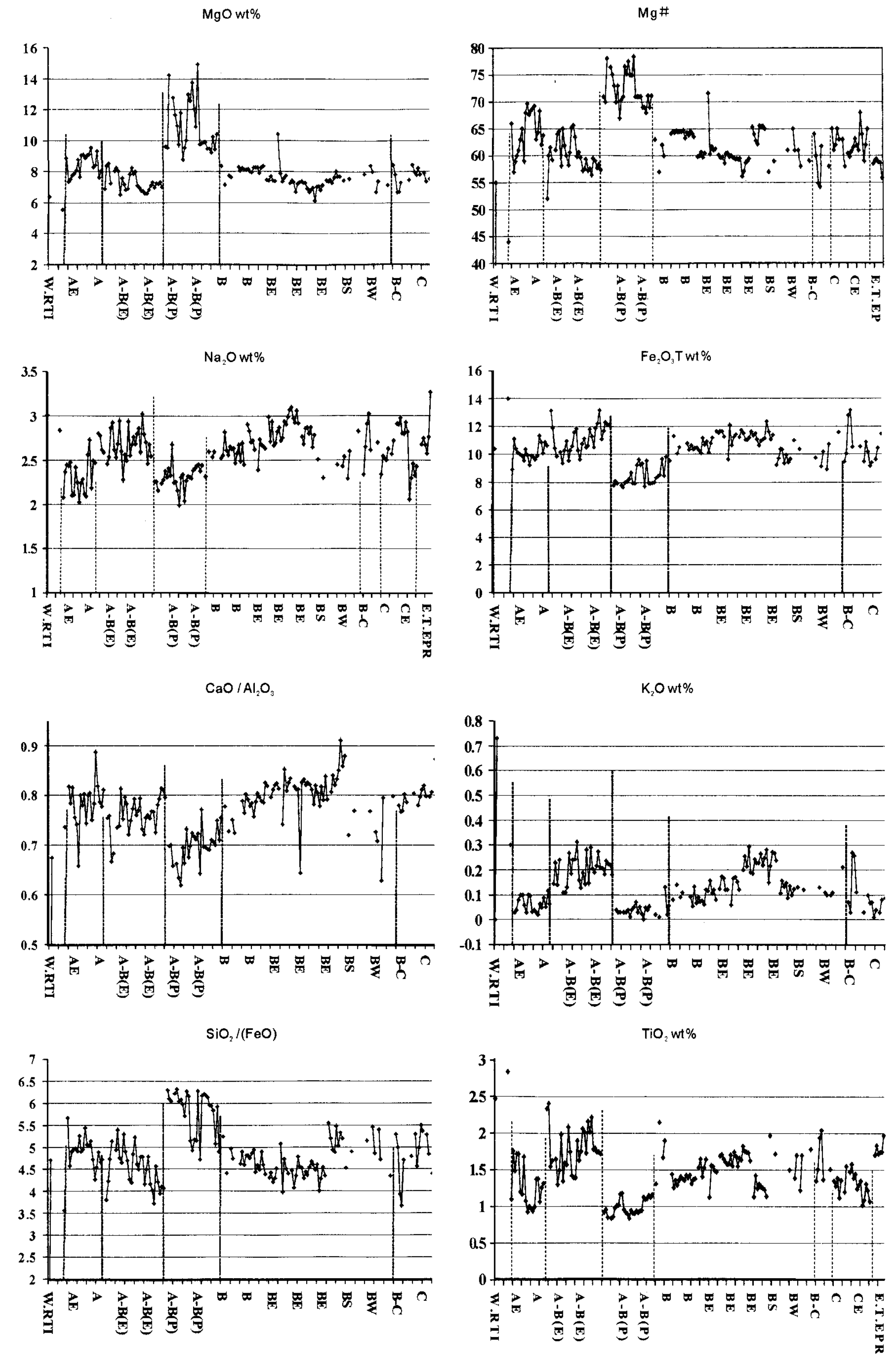

Fig. 2 Basalt major element compositions vs. tectonic settings

图2 玄武岩主要元素成分及其对应的构造环境

W.RTI: western ridge-transform intersection; AE: eastern part of spreading center A; BE, BS, BW: eastern, southern and western part of spreading center B, respectively; other symbols refer to Fig. 1

ITSC A: Samples from A have Zr contents of $(40 \sim 122) \times 10^{-6}$, Sr contents of 58 ~ 121, and Cr contents of 176 ~ 438 (most >300 × 10^{-6}). The incompatible element ratios of Zr/Y, Ti/Zr and K/Ti are 1.69 ~ 3.20, 85.62 ~ 148.49, and 0.03 ~ 0.12, respectively. Basalts are LREE-depleted, having REE concentrations of 10 ~ 20 times of chondrite with un-fractionated heavy REE abundances and (La/Yb)cn ratios of 0.31 ~ 0.78, (Ce/Yb)cn ratios of 0.72 ~ 1.01, and (La/Sm)cn ratios of 0.37 ~ 0.75.Most are typical N-MORB, and some of them are more primitive N-MORB (Table 3, Fig. 3).

ITSC B: Basaltic rocks in spreading center B appear very diverse, having Zr contents of $(62 \sim 157) \times 10^{-6}$ (most are $(65 \sim 115) \times 10^{-6}$), Cr contents of $(190 \sim 430) \times 10^{-6}$ (two groups: one ranges from 190×10^{-6} to 280×10^{-6}, the other ranges from 330×10^{-6} to 430×10^{-6}), Sr contents of $95 \times 10^{-6} \sim 137 \times 10^{-6}$, Ni contents of $40 \times 10^{-6} \sim 300 \times 10^{-6}$. Their ratios of Zr/Y, Ti/Zr and K/Ti are 2.17 ~ 3.78, 82.11 ~ 122.33, and 0.05 ~ 0.26, respectively. The basalts appear LREE- depleted to weakly LREE-enriched, most $(La/Yb)_{cn}$ ratios range from 0.46 ~ 0.66, and some are 0.67 ~ 0.86, and the $(La/Sm)_{cn}$ ratios have a similar variation: most are of 0.40 ~ 0.59, some 0.62 ~ 0.77. They are typical N-MORBs. (Table 3, Fig. 3).

ITSC C and D: Basalts from C have Zr contents of $71 \sim 95 \times 10^{-6}$, Cr contents of $(190 \sim 425) \times 10^{-6}$, Sr contents of 100 ~ 115, and Ni contents of 25 ~ 60. The ratios of Zr/Y, Ti/Zr and K/Ti are 2.42 ~ 3.21, 90 ~ 117, 0.05 ~ 0.14, respectively. Their REE patterns are similar to B with (La/Yb)cn ratios of 0.45 ~ 1.02 and $(La/Sm)_{cn}$ ratios of 0.45 ~ 0.93. The compositions from D are similar to C with Zr content of $(59 \sim 77) \times 10^{-6}$, Cr content of $(285 \sim 430) \times 10^{-6}$, Ni content of $(35 \sim 85) \times 10^{-6}$, Sr contents of 91 ~ 111. The ratios of Zr/Y, Ti/Zr and K/Ti are 2.30 ~ 2.93, 87.45 ~ 111.52, 0.05 ~ 0.10. Their REE patterns are LREE-depleted with $(La/Yb)_{cn}$ ratios of 0.46 ~ 0.79 and $(La/Sm)_{cn}$ ratios of 0.46 ~ 0.79, and are typical N-NORBs (Table 3, Fig. 3).

Strike-slip fault A-B (E)(evolved): The fractionated samples from A-B have enriched incompatible elements with Zr contents of$(72.9 \sim 165.00) \times 10^{-6}$, Cr contents of $(199.32 \sim 395.93) \times 10^{-6}$, Sr contents of $(101 \sim 133.34) \times 10^{-6}$, and Ni contents of $(52 \sim 198) \times 10^{-6}$. Their incompatible element ratios of Zr/Y, Ti/Zr and K/Ti are 2.4 ~ 4.25, 80.52 ~ 114.8, 0.08 ~ 0.23, respectively. The REE patterns of most samples are LREE-depleted with $(La/Yb)_{cn}$ ratios of 0.53 ~ 0.89 and $(La/Sm)_{cn}$ ratios of 0.49 ~ 0.77, and are typical N-MORBs (Table 3, Fig. 3).

Strike-slip fault A-B (P): The primitive samples from A-B have very low incompatible element concentration with Zr contents of $(32 \sim 75) \times 10^{-6}$, Sr contents of $(54.1 \sim 84) \times 10^{-6}$, Cr contents of $(440 \sim 1470) \times 10^{-6}$ (most range from $(450 \times 10^{-6}$ to $1\,000 \times 10^{-6})$, and Ni content of $(185 \sim 831) \times 10^{-6}$ (most are $200 \times 10^{-6} \sim 400 \times 10^{-6}$). The ratios of Zr/Y, Ti/Zr and K/Ti are 1.6 ~ 3.13 (most are 1.8 ~ 2.5), 95.1 ~ 143.3, 0.02 ~ 0.08. LREE are strongly depleted with (La/Yb)cn ratios of 0.20 ~ 0.51, (La/Sm)cn ratios of 0.20 ~ 0.47, and are very primitive N-MORBs (Table 3, Fig. 3).

Strike-slip faults B-C and C-D: Basalts from fault B-C have Zr contents of $(63 \sim 127) \times 10^{-6}$, Cr contents of$(151 \sim 310) \times 10^{-6}$, Ni contents of$(40 \sim 70) \times 10^{-6}$, and Sr contents of $(88 \sim 125) \times 10^{-6}$. The ratios of Zr/Y, Ti/Zr and K/Ti are 2.14 ~ 2.84, 92.86 ~ 129.35, 0.05 ~ 0.18, respectively. The REE patterns are LREE-depleted, with (La/Yb)cn ratios of 0.44 ~ 0.73, (La/Sm)cn ratios of 0.44 ~ 0.78. Only one sample is available from C-D fault, and has Zr content of 67×10^{-6}, Cr content of 450×10^{-6}, Ni content of 170×10^{-6} and Sr content of 112×10^{-6}. Its REE pattern is LREE depleted with (La/Yb)cn ratio of 0.78 and (La/Sm)cn of 0.78, and all of them are N-MORBs (Table 3, Fig. 3).

Eastern Tip of EPR: Basaltic rocks from this region have Zr contents of $105 \times 10^{-6} \sim 117 \times 10^{-6}$, Cr contents of $(205 \sim 290) \times 10^{-6}$, Ni contents of $(60 \sim 105) \times 10^{-6}$, Sr contents of $(113 \sim 124) \times 10^{-6}$. The ratios of Zr/Y, Ti/Zr and K/Ti are 2.8 ~ 3.28, 5.40 ~ 101.43, 0.08 ~ 0.20. REE pattern are LREE depleted with $(La/Yb)_{cn}$ ratios of 0.53 ~ 0.68 and (La/Sm)cn ratios of 0.44 ~ 0.67. These basalts are N-MORBs (Table 3, Fig. 3).

3.2 Variations of trace and rare-earth element geochemistry within the transform

K/Ti, $(La/Yb)_{cn}$, $(La/Sm)_{cn}$ ratios and rare-earth element compositions can be used to infer mantle source characteristics, and delineate depleted (lower ratios) from enriched (higher ratios) source domain. Three classes of MORBs are distinguished in the transform domain.

E-MORBs: The REE compositions of the western ridge-transform intersection (W.RTI) basalts are

Table 3 REE Composition Summary

表3 稀土元素成分一览

SETTINGS	STAT	La	Ce	Nd	Sm	Eu	Gd	Dy	Y	Er	Yb
A											
(11)*	Avg	7.7631	12.6793	12.4461	15.4115	16.7757	17.911	17.4114	17.0652	17.6936	15.1335
	Min	4.2034	9.4348	7.3023	11.4348	13.7033	15.8035	14.9753	14.6624	14.8327	13.4184
	Max	14.1232	17.8527	19.6661	18.9104	20.8293	20.4528	20.3609	19.5054	20.5988	18.1368
A-B(E)											
-24	Avg	15.2523	21.0417	25.7472	24.0875	24.438	24.9646	24.308	24.5119	25.4958	21.592
	Min	9.8742	14.462	18.1283	15.9594	19.4989	17.466	16.6944	16.5732	17.8858	15.9793
	Max	19.5403	25.9449	32.9411	30.9396	29.6307	31.7288	30.607	31.8579	32.56	28.1848
A-B(P)											
-8	Avg	4.9652	9.626	11.287	13.5598	15.0982	16.1209	14.4497	14.6333	14.6888	12.3295
	Min	2.2856	7.2024	9.443	9.9153	11.848	13.3992	12.9491	12.9922	13.1433	10.5369
	Max	7.1644	12.3278	12.4514	15.7061	17.0773	21.3286	16.8346	17.4054	17.2767	13.9357
B											
-51	Avg	11.4152	17.4528	20.4974	20.8995	21.8202	22.1068	21.428	20.9347	22.099	18.9066
	Min	7.1135	13.8667	14.8682	13.5692	16.2179	17.9311	17.916	16.8103	17.4735	14.3172
	Max	16.3626	21.1019	27.5415	27.1559	26.9758	27.8246	25.6297	25.317	26.7671	22.7028
B-C											
-3	Avg	14.3447	21.6395	25.7601	21.5478	24.2857	25.7656	26.3419	25.2458	26.548	22.0697
	Min	8.5138	15.3328	18.1936	13.8564	17.8446	19.9843	19.9315	18.9919	19.5363	16.4854
	Max	17.9509	25.6437	30.6445	27.6892	28.9878	29.0203	29.806	28.7672	31.7093	25.236
C											
-6	Avg	11.3424	17.1025	18.1187	20.4343	22.0984	22.3338	21.086	20.3506	20.4189	18.8712
	Min	8.6773	14.9206	15.9515	18.8786	20.2278	20.2197	19.8925	18.9784	19.4916	17.7101
	Max	13.7061	18.5766	20.8232	22.636	23.7112	23.9982	22.3016	21.6598	21.3454	20.051
D											
-1		9.5896	15.4573	16.1195	12.8819	14.8746	17.0013	16.4576	16.0454	16.7688	14.0528
E.T.EPR											
-6	Avg	12.4587	20.2804	25.2961	25.8065	25.2173	26.1652	24.7876	23.8305	23.7464	22.2176
	Min	10.4407	17.9758	22.2907	23.543	22.6674	23.029	22.3629	21.5897	21.754	19.6642
	Max	14.4674	22.1051	27.4846	27.1252	27.3071	28.2306	26.6593	25.3423	24.951	24.1229
W.RTI											
-5	Avg	50.6104	47.7338	40.7896	32.5844	29.6018	27.7944	24.564	23.1248	23.6222	20.2122
	Min	16.672	21.626	25.231	25.09	24.6429	24.713	24.015	22.401	22.671	19.228
	Max	61.095	55.479	45.254	36.03	31.3929	29.156	25.185	23.488	24.985	21.218

*number of samples; REEs were normalized by the chondrite value

markedly different from basalts from other tectonic locations. As shown in Fig. 2, samples from W.RTI have the highest ratios of $(La/Yb)_{cn}$ and $(La/Sm)_{cn}$ (2.82 ~ 3.14, 1.70 ~ 1.93, respectively) and are the most fractionated basalts (E-MORBs) in the transform domain. They also have the highest contents of Zr (>170 × 10^{-6}) and Sr (>270 × 10^{-6}) and highest Zr/Y ratios (> 5.0). Other samples from W.RTI have intermediate ratios with $(La/Yb)_{cn}$ of 0.79 ~ 0.87 and $(La/Sm)_{cn}$ of 0.66 ~ 0.76, and they are normal MORB with elevated REE concentrations.

Primitive N-MORBs: The most primitive N-MORBs are from the strike-slip fault A-B in this domain with the lowest ratios of $(La/Yb)_{cn}$ (0.20 ~ 0.51) and $(La/Sm)_{cn}$ (0.20 ~ 0.47). There are also some primitive basalts from spreading centers A, rarely from C and D. They all have the lowest contents of Zr, Sr, and Ti, the lowest ratios of Zr/Y and K/Ti, and the highest contents of Ni and Cr and high Ti/Zr ratios.

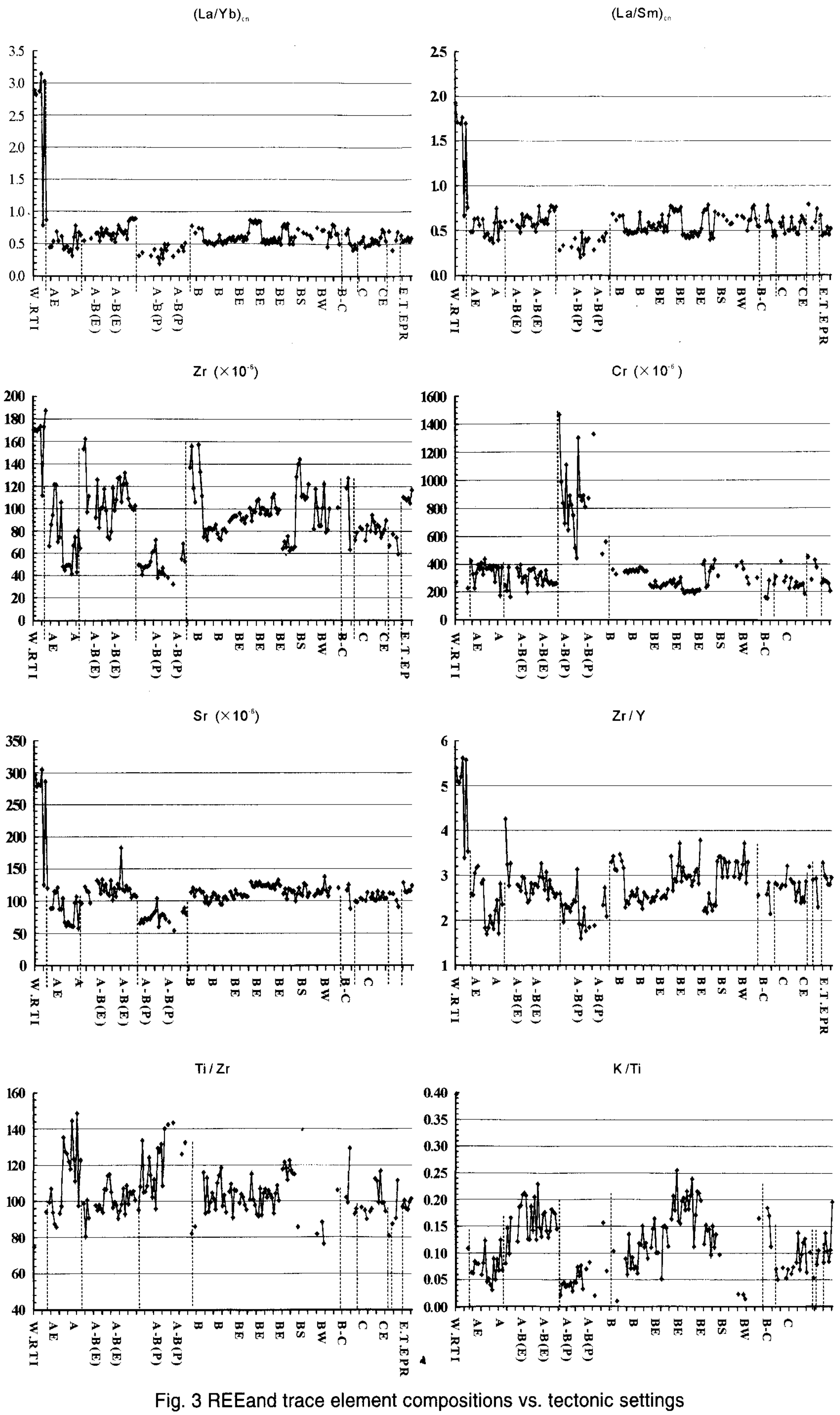

Fig. 3 REEand trace element compositions vs. tectonic settings

图 3 稀土和微量元素成分及与之对应的构造环境

W.RTI: western ridge-transform intersection; AE: eastern part of spreading center A; BE, BS, BW: eastern, southern and western part of spreading center B, respectively; other symbols refer to Fig. 1

N-MORBs: Most samples from spreading center B and western section (fault B-C, spreading centers C and D, and E.T.EPR) of the domain, some samples from fault A-B, and spreading center A, have intermediate to high incompatible and rare-earth element contents and incompatible element ratios, and they are typical N-MORBs. As shown in the extended REE plots, most basalts show negative Sr anomalies except samples from A-B (Primitive) with Sr anomalies of 1. Ti anomalies have similar variations.

4 Discussions

4.1 Mantle source tracers

Previous studies of MORBs have recognized that the suboceanic mantle is heterogeneous on various scales (Hart, 1984, 1988; White and Hoffman, 1992; Zindler et al., 1984). Incompatible trace elements ratios, $^{87}Sr/^{86}Sr$, $^{143}Nd/^{144}Nd$, and common lead isotopic ratios provide evidence of source heterogeneity (Schilling et. al., 1983; Langmuir, 1994; Holness and Richter, 1989; Hart, 1988; White et al., 1993). However, incompatible trace element ratios do not uniquely indicate source heterogeneity because they change with the extent of partial melting. Isotopic ratios of Sr, Nd, and Pb record the characteristics of the source region for "zero age" MORBs. These ratios are not affected by either degree of partial melting or fractional crystallization. Therefore, they provide more reliable means to define mantle source heterogeneity. Combined incompatible trace element ratios and isotopic ratios can provide better constraints on the nature of the source region heterogeneity.

Rare-earth elements have very similar chemical and physical properties because they all have similar atomic structures. The differences that do exist in chemical behavior are a result of the small but steady decrease in atomic (and ionic) radii from La to Lu (Rollinson, 1993). These small differences in size and chemical behavior cause them to be fractionated relative to each other by various petrologic and mineralogical processes.

The REE are regarded as amongst the least soluble trace elements, and the REE patterns can faithfully represent the original composition of the unaltered parent rocks (Rollinson, 1993). They also help to define the compositional heterogeneity within the mantle. From a geochemical perspective, the mantle can be divided into three parts: mantle lithosphere, the source of MORB (depleted mantle) and the source of mantle plumes. The shapes of REE patterns are influenced by the shapes of the mineral-melt distribution coefficient patterns of the minerals in the residual melt. Most mid-ocean ridge basalts (MORBs) exhibit a light rare earth-depleted pattern, which reflects the incompatible element-depleted nature of the upper mantle from which these magmas are derived. MORB can further be divided into three types: E-MORB (incompatible element-enriched) or P-MORB (mantle plume) and N-MORB (normal) based on their geochemical differences.

Fractional crystallization involving olivine, plagioclase, clinopyroxene and spinel increases the total REE content of more evolved MORB, but does not produce any significant inter-element fractionation. The characteristic shape of the primary basalt REE patterns is maintained in the more evolved basalts. However, there is a tendency for a negative Eu anomaly to develop as fractionation proceeds, because Eu is preferentially partitioned into plagioclase. If partial melting is fairly extensive (>10%) the REE should not be fractionated from each other during partial melting and therefore ratios of REE (e.g. La/Sm, La/Yb and La/Ce) should reflect the ratios in the mantle source of the magmas. However, only the very light REE are truly incompatible and thus, of the ratios above, only La/Ce is likely to be diagnostic of source composition

4.2 Possible mantle sources beneath Siqueiros transform

In the Siqueiros transform area, some important trace and rare earth elemental characteristics and their variations (Table 3; Fig. 3 and Fig. 4) have been recognized. No new isotopic samples have been analyzed in this study, but published and unpublished isotopic data from this area and the nearby East Pacific Rise are available. Two different MORB mantle sources have been identified.

Enriched mantle: the source of the enriched MORB in the western ridge-transform intersection area. The basalts from this source are characterized by strongly LREE-enriched REE pattern (Fig.4).They have the lowest MgO contents (5.54 ~ 6.37 wt%) and highest TiO_2 (2.47 ~ 2.84 wt%) and highest K_2O contents (0.3 ~ 0.73 wt%) in the study area. As shown in Fig. 2 and Fig. 3, rocks from W.RTI have the highest ratios of $(La/Yb)_{cn}$, $(La/Sm)_{cn}$ and Zr/Y (2.82 ~ 3.14, 1.70 ~ 1.93, 3.4 ~ 5.6, respectively) and are the most fractionated basalts in this

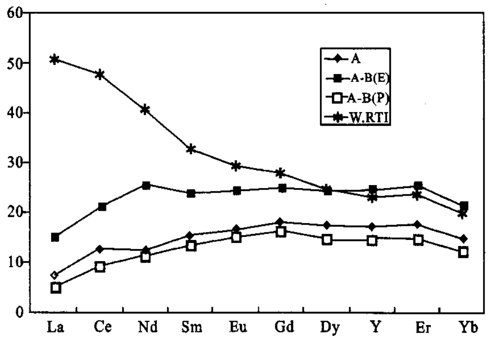

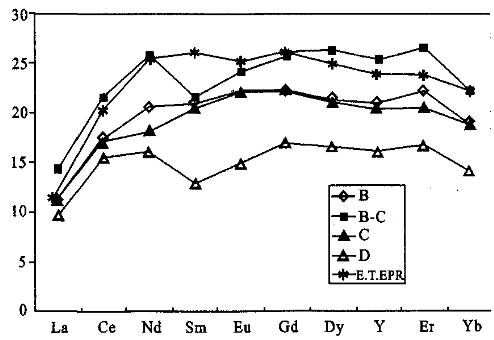

Fig. 4 Averaged REE patterns of MORBs from Siqueiros transform area

图 4 Siqueiros 转换断层区洋中脊玄武岩的稀土元素图谱

Most samples from western ridge–transform intersection have enriched LREE, high REE concentrations, and imply an enriched mantle source. Samples from fault A–B (primitive) and some samples from spreading center A have LREE–depleted REE patterns, and low REE concentrations (10 ~ 20 times of chondrite REE); Most samples from middle–eastern domain (including spreading centers B, C and D, faults B–C and C–D, nearby eastern East Pacific Rise, and some samples from A–B and A) are light LREE–depleted with 20–30 times of chondrite REE concentrations

transform domain. They also have the highest contents of Zr (>170× 10^{-6}), and Sr (>270 × 10^{-6}), and highest Zr/Y ratios (>5.0). The Sr isotopic compositions of two of those basalts from this area ($^{87}Sr/^{86}Sr$ = 0.702 89, Macdougal and Lugmair,1986); $^{87}Sr/^{86}Sr$ = 0.702 99, Casey's unpublished data) indicate that its source is enriched relative to normal N-MORB mantle beneath Siqueiros.A sample from the nearby northern East Pacific Rise has similar $^{87}Sr/^{86}Sr$ ratio (0.7029, R13-1) (Carlson et al., 1978), implying that this mantle source extends to the norther side of the EPR (south of EPR at 10° 30').

Depleted mantle: the source of the basalts from the transform domain, including primitive N-MORBs from fault A-B and spreading center A, and all other normal N-MORBs.These samples are characterized by intermediate to highest contents of MgO (6.0 ~ 14.91 wt%), Na_2O (2.16 ~ 3.0 wt%), TiO_2 (0.84 ~ 2.4 wt%) and K_2O (0.0013 ~ 0.30 wt%) (Table 2 and Fig.2). They have slight to strong LREE-depleted REE patterns ($(La/Yb)_{cn}$ = 0.20 ~ 0.90 and $(La/Sm)_{cn}$ = 0.20 ~ 0.80)). They also have the intermediate to lowest contents of Zr, Sr, Ti, intermediate to lowest ratios of Zr/Y, K/Ti, intermediate to highest contents of Ni, Cr and Ti/Zr ratios. The Sr isotopic compositions of four primitive samples from fault A-B are lower and have narrow variations ($^{87}Sr/^{86}Sr$ = 0.702 59 ~ 0.702 61, Casey's unpublished data). Normal N-MORBs from EPR at 10° 30' (Regelous et al., 1999) and southern EPR between 13° ~ 23° (Mahoney et al., 1994) have Sr isotopic ratios of 0.702 47 ~ 0.702 68, and 0.702 4 ~ 0.702 7, respectively. The isotopic ratios of basalts from fault A-B are in the range of sample from neaby nomal EPR basalts, and this implies that these basalts are all from a highly "depleted" reservoir of material in the mantle.

5 Conclusions

This study examined geochemical characteristics and mantle source heterogeneity at Siqueiros transform and the nearby East Pacific Rise. Major element, trace element and REEs of basalts recovered from this area were analyzed using ICP Spectrometer during this study.

Basalts from the Siqueiros transform exhibit a wide compositional range from primitive to evolved compositions. Three classes of MORBs are distinguished in the transform domain: 1) E-MORBs: Basalts from the western ridge-transform intersection (W.RTI) are markedly different from basalts from other tectonic locations. They have lowest MgO contents of 5.54 ~ 6.37 wt%; highest Na_2O contents (2.84 ~ 3.27 wt%); lowest CaO/Al_2O_3 ratio (< 0.70); highest ratios of $(La/Yb)_{cn}$ (2.82 ~ 3.14) and $(La/Sm)_{cn}$ (1.70 ~ 1.93) and Zr/Y ratios (>5.0); and highest contents of Zr (>170× 10^{-6}) and Sr (>270× 10^{-6}). 2) Primitive N-MORBs: Samples from A-B, and some samples from A are the most primitive basalts in this area. They have highest Mg values of 67 ~ 78 and highest MgO contents up to 14.91 wt% and lowest Na_2O contents (1.99 ~ 2.50 wt%); lowest ratios of

$(La/Yb)_{cn}$ (0.20 ~ 0.47), $(La/Sm)_{cn}$ (0.20 ~ 0.47), Zr/Y and K/Ti; lowest contents of Zr, Sr, and Ti, and the highest contents of Ni and Cr; and high Ti/Zr ratios. 3) N-MORBs: Samples from A-B, some samples from A, most samples from B and western section (B-C, C, D and E.T.EPR) of the domain have intermediate to high incompatible and rare-earth element contents and incompatible element ratios, and they are typical N-MORBs.

Two mantle sources exist in the Siqueiros region. One is the enriched mantle with highest REEs, enriched LREEs, low MgO, K_2O and TiO_2 and high $^{87}Sr/^{86}Sr$ isotopic concentrations, which lies underneath the western part of the transform domain. The second source is the depleted mantle, which lies underneath the mid-eastern transform domain. Basalts from this source have low $^{87}Sr/^{86}Sr$ isotopic compositions, lower REEs and trace elements and higher MgO contents.

Reference:

[1]Anders and Grevesse, Abundances of the elments: Meteoritic and solar. Geochimica et Cosmochimica Acta. Vol. 53, pp. 197-214. 1989

[2]Bender, J. F, C. H. Langmuir, Evidence from the Tamayo region of the EPR for a transform fault effect on basalt chemistry. Eos, Transactions, American Geophysical Union. 64; 18, Pages 332. 1983.

[3]Bonatti, E., and J. Honnorez, Sections of the Earth's crust in the equatorial Atlantic. Ibid. 81, 4104-16, 1976.

[4]Bryan W. B., Thompson G., Frey F. A. And Dickey J. S., Inferred geologic settings and differentiation in basalts from the Deep-Sea Drilling Project, J. Geophys. Res., 81, 4285-4304, 1976.

[5]Carlson, R. W., J. D. Macdougall and G. W. Lugmair, Differential Sm-Nd evolution in oceanic basalts, Geophys. Res. Lett. 5, 229-232, 1978.

[6]Detrick R. S., and Purdy G. M., The crustal structure of the Kane Fracture Zone from seismic refraction studies, J. Geophys. Res.85, 3759-3777, 1980.

[7]Fox P. J., The effect of transform faults on the character of ocean crust. Abstr. Progrm. Geol.Soc. Am., 7, 403, 1978.

[8]Fox P. J., R.S. Detrick and G.M. Purdy, Evidence for crustal thinning near fracture zones: implications for ophiolites. Proc. Int. Ophiolite Symp. Cyprus, 161-8, 1981.

[9]Fox P. J, Gallo D. G., Madsen J. A., Macdonald K. C., The use of Seabeam to elucidate the morphotectonic elements of fast-slipping transform boundaries.In: American Geophysical Union; 1984 ocean sciences meeting. Eos, Transactions, American Geophysical Union. 64; 52, Pages 1031. 1983.

[10]Gallo D. G., and P.J. Fox, The influence of transform faults on the generation of oceanic lithosphere. Eos, Transactions, American Geophysical Union, 1979, 60, 376.

[11] Hart S. R., A large-scale isotope anomaly in the southern hemisphere mantle, Nature, 309, 753-757, 1984.

[12] Hart S. R., Heterogeneous mantle domains: Signature, genesis and mixing chronologies, Earth Planet. Sci. Lett., 90, 273-296, 1988.

[13]Hekinian, R. and G.Thompson, Comparative geochemistry of volcanics from rift valleys, transform and aseismic ridges. Contr. Miner. Petrol. 57, 145-162, 1976.

[14]Holness, M.B., and F.M. Richter, Possible effects of spreading rate on MORB isotopic and rare earth composition arising from melting of a heterogeneous source. J. Geol., v.97, 247-260. 1989.

[15]Langmuir C. H., Major element heterogeneity in the mantle; constraints from a general model for basalt petrogenesis. Mineralogical Magazine. 58A; L-Z, Pages 511-512. 1994.

[16]Langmuir C. H., Petrology database, vol. 2and vol.3, Joint Oceanographic Institutions, washington, D. C., 1988.

[17]Langmuir C. H., J. F. Bender, the geochemistry of oceanic basalts in the vicinity of transform faults: observations and implications, Earth Planet. Sci. Lett. 69, 107-127, 1994.

[18]Langmuir, C. H., Klein E. H., and Plank, Petrological systematics of mid-ocean ridge basalts: constraints on melt generation beneath ocean ridges, In: Mantle Flow and Melt Generation at mid-Ocean Ridges, Geophys. Monogr. Ser., vol. 71. J. Phipps Morgan and Blackman D.K., and Sinton, J.M., (editors), pp. 183-280, AGU, Washington, D.C., 1992.

[19]le Roex, A.P., Dick, H.J.B., Erlank A.J., Reid, A.M., Frey, F.A., and Hart, S.R., Geochemistry, mineralogy and petrogenesis of lavas erupted along the Southwest Indian Ridge between the Bouvet Triple Junction and 11 degrees East, J. Petrol., 24, 267-318, 1983.

[20]le Roex, A.P., Dick, H.J.B., Reid, A.M., Frey, F.A., Erlank A.J., and Hart, S.R., Petrology and geochemistry of basalts from the American-Antarctic Ridge, southern Ocean: implications for the westward influences of the Bouvet mantle plume, Contrib. Mineral. Petrol., 90, 367-380, 1985.

[21Macdougal, J. D. & Lugmair, G. W. Sr and Nd isotopes in basalts from the East Pacific Rise: significance for mantle heterogeneity, Earth planet Sci. Lett. 77, 273?284, 1986.

[22]Mahoney, J. J.; Sinton, J. M., Kurz, M. D., MacDougall, J. D., Spencer, K. J., Lugmair, G. W., Isotope and trace element characteristics of a super-fast spreading ridge: East Pacific rise, 13-23° S, Earth and Planetary Science Letters, Volume 121,

Issue 1-2, p. 173-193, 1994.

[23] Melson, W.G., G. Thompson, Petrology of transform fault zones and adjacent ridge segments. Phil. Trans.R. Soc. Lond. A268, 37-70, 1971.

[24] Perfit M. R., Fornari D. J., Ridley W. I., Kirk P. D., Casey J., Kastens K. A., Reynolds J. R., Edwards M., Desonie D., Shuster R., Paradis S., Recent volcanism in the Siqueiros transform fault; picritic basalts and implications for MORB magma genesis. Earth and Planetary Science Letters. 141; 1-4, 91-108. 1996.

[25] Regelous, et al., Variations in the geochemistry of magmatism on the East Pacific Rise at 10o30' N since 800 ka. Earth and Planetary Science Letters, Vol. 168, pp. 45-63, 1999.

[26] Rollinson, H., Using Geochemical Data: Evaluation, presentation, interpretation. Longman Singapore Publishers (Pte) Ltd., Singapore. 1993.

[27] Schilling, J. G., Rare-earth variations across 'normal segments' of the Reykjanes ridge, 60° -53° N, mid-Atlantic ridge, 29° S, and East Pacific rise, 2° -19° S, and evidence on the composition of the underlying low-velocity layer. Journal of Geophysical Research, Vol. 80, Issue B11, p. 1459-1473, 1975.

[28] Schilling, J. G.; Zajac, M.; Evans, R.; Johnston, T.; White, W.; Devine, J. D.; Kingsley, R. Petrologic and geochemical variations along the Mid-Atlantic Ridge from 29° N to 73° N. American Journal of Science, 283(6), 510-86, 1983.

[29]Smith, S.E., Geochemistry and petrology of basaltic and plutonic rocks from the Hayes Transform region, Mid-Atlantic Ridge, Ph.D. dissert., University of Houston, TX, 1994.

[30] Stroup, J.G., and P.J. Fox, Geologic investigations in the cayman Trough: Evidence for the thin crust along the mid-Cayman rise. J. Geol., 89, 243-258, 1981.

[31] Sun. S.S., R.W. Nesbitt, and A.Y. Sharaskin, Geochemistry characteristics of mid-ocean ridge basalts, Earth Planet. Sci. Lett., 44, 119-138, 1979.

[32] White, W. M., and A.W. Hoffman, Sr and Nd isotope geochemistry of oceanic basalts and mantle evolution, Nature, 296, 821-825, 1992.

[33] White, W.M., A.R. McBirney, and R.A. Duncan, Petrology and geochemistry of the Galapagos Islands: Portrait of a pathological mantle plume. J. geophys. Res., v.98(B), 19533-19563, 1993.

[34] Zindler et al., Isotope and trace element geochemistry of young Pacific seamounts: implications for the scale of upper mantle heterogeneity, Earth Planet. Sci. Lett., 70, 175-195; 1984.

东太平洋洋隆 Siqueiros 转换断层带的地球化学特征

颜耀阳, John F Casey

（南佛罗里达州水资源管理署，美国佛罗里达西棕榈海滩，FL 33406;
休斯顿大学地球科学系，美国得州休斯顿, TX 77204）

摘 要: 东太平洋洋隆 Siqueiros 转换断层带（西经 103° ~ 104° 、北纬 8° 20′ ~ 8° 30′ ），位于中美洲之西可可斯板块与太平洋板块交接处（图 1）。该转换断层的玄武岩，成分从原始的到富化的，变化很大。最原始的玄武岩产于 A-B 走滑断层内，其 MgO 含量高达 14.91 %；最富化的玄武岩产在西部洋脊与转换断层交叉部位，其 MgO 含量较低，成分变化大。转换断层内的洋中脊玄武岩可分三类：富化的洋脊玄武岩(E-MORB)、原始的正常洋脊玄武岩(Primitive N-MORB) 和正常洋脊玄武岩 (N-MORB)。Siqueiros 转换断层区已确定有两个地幔源：一个位于转换断层西部下面的富集地幔，其特点是稀土总量高，富轻稀土，低 MgO、K_2O 和 TiO_2，而高 $^{87}Sr/^{86}Sr$；另一个是位于转换断层中 - 东部下面的亏损地幔，来自这个地幔源的玄武岩具有低 $^{87}Sr/^{86}Sr$、低稀土元素和微量元素含量，但 MgO 含量较高。

关键词: 洋中脊玄武岩；地球化学；地幔追踪；Siqueiros 转换断层；东太平洋洋隆

后语: 白瑾先生德高望重，是我(第一作者)如父亲般的师长。自 1987 年荣幸地成为白先生的研究生后，即追随先生北上辽东，西进中条，横跨秦岭，所获知识受益终生。十年前旅美至今，亦时时得到白先生的指导与关心。白先生在科研上严谨，生活上淡泊，一直是我学习的楷模。仁者寿，值此先生八十华诞之际，衷心祝愿先生健康长寿!